

Electronic correlations and screening effects in the Hund’s polar metal SrEuMo₂O₆

Gianluca Giovannetti,^{1,*} Danilo Puggioni,² James M. Rondinelli,^{2,†} and Massimo Capone¹

¹*CNR-IOM-Democritos National Simulation Centre and International School
for Advanced Studies (SISSA), Via Bonomea 265, I-34136, Trieste, Italy*

²*Department of Materials Science and Engineering Northwestern University 2220 Campus Drive, Evanston, IL 60208-3108, USA*

Using a first-principles approach based on density functional theory and dynamical mean field theory, we study the electronic properties of a new candidate polar metal SrEuMo₂O₆. Its electronic structure shares similarities with centrosymmetric SrMoO₃ and EuMoO₃, from which it may be considered an ordered derivative, but ferroelectric-like distortions of the divalent cations and oxygen anions lift inversion symmetry mediated by an anharmonic lattice interaction in the metallic state. We find that Hund’s coupling promotes the effects of electronic correlations owing to the Mo⁴⁺ *d*² electronic configuration, producing a correlated metallic phase far from the Mott state. The conundrum between metallicity and polar distortions is thereby alleviated through the renormalized quasiparticles, which are unable to fully screen the ordered local dipoles.

PACS numbers: 75.85.+t, 71.20.-b, 71.45.Gm, 77.80.B-, 78.20.Ci

“Ferroelectric metals” are emerging as a new paradigm in condensed matter physics from which exotic phenomena can be discovered and new technology platforms established [1]. The possible existence of these materials was predicted theoretically a half century ago [2], but a conclusive observation of an intrinsic metallic material which undergoes an inversion-symmetry lifting (polar) transition has been obtained only recently in LiOsO₃ [3]. The theoretical appeal of these materials lies in the contrast with one’s intuition: Itinerant electrons in metals are expected to screen electric fields and to inhibit long-range Coulomb interactions from cooperatively ordering ferroelectric-like displacements [4–6]. It is therefore uncommon and surprising to find metals that undergo the same structural transitions that occur in isostructural and insulating analogues; it is this incompatibility, in part, that explains the scarcity of polar non-centrosymmetric metals (NCSM).

Nonetheless, polar displacements and metallicity can coexist provided that the ferroelectric-like distortions are largely decoupled from the electronic structure at the Fermi level, *i.e.*, the electrons responsible for transport [2, 7]. This appears to be the main operational principle active in oxide-based NCSM: LiOsO₃ [3] exhibits a second-order displacive transition from a non-polar to polar structure (crystal class *C*_{3*v*}) with displacements of Li and O rather than Os, whose orbitals are responsible for the metallic behavior [8]; LaSr₂Cu₂GaO₇ has a polar structure (*C*_{2*v*}) owing to the presence of intrinsically acentric tetrahedral GaO₄ units, whereas the conduction band is mainly of copper character [9, 10], and Cd₂Re₂O₇ is a geometrically frustrated pyrochlore that becomes optically active (*D*_{2*d*}) as oxygen rather than Re displacements lift inversion symmetry below 200 K [11, 12].

Although the framework described in Ref. 7 provides a *structural* understanding for the stability of oxide and non-oxide NCSM, it is partially limited, as it considers all metallic states equivalent assuming a Fermi liquid description. Yet, the rich phenomenology of *strongly correlated*

oxides demonstrates that strong electron-electron interactions can lead to metallic states which challenge the Landau Fermi-liquid paradigm. Anomalous metallic states range from non-Fermi-liquid metals, with unconventional scaling behavior of the resistivity and other observables, to ‘bad’ metals that retain Fermi-liquid coherence only below a very low coherence temperature, above which the Mott-Ioffe-Regel limit breaks [13]. More recently the possibility of a ‘bad metal’ far from the Mott-Hubbard localization state has been proposed in the presence of a sizable Hund’s coupling [14, 15].

Therefore, we pose the question: How does the nature of the metallicity dictate the compatibility between inversion lifting displacements and ‘delocalized’ electrons? The crucial and non-trivial role of the quasiparticle character on screening of the long-range Coulomb interactions may be gleaned from recent studies on electron doped BaTiO₃ [16, 17]: Optical conductivity measurements show spectral weight shifts with carrier concentration [18] that are accompanied by a decrease in the ferroelectric-like distortion across the doping-driven insulator-metal transition.

As a starting point, we first discuss the previously mentioned NCSM oxides within this context. Indeed all may be considered to exhibit strong electron correlations. The residual resistivity in LiOsO₃ is larger than that expected for a normal metal and the magnetic susceptibility displays a Curie-Weiss component suggesting an incipient localization of the carriers [3]. LaSr₂Cu₂GaO₇ shares the same Cu-O planar structure of YBa₂Cu₃O₇, one of the most studied cuprate superconductors for which strong deviations from the Fermi-liquid paradigm are well established [19]. Optical studies of Cd₂Re₂O₇ reveal an exotic metallic state with strong mass renormalizations [20]. Lastly, a recent theoretical proposal identifies NCSM in ultra-short superlattices of SrRuO₃ and CaRuO₃ [7], two compounds displaying strong correlations due to the Hund’s coupling [21].

Although the role of strong correlations in compounds

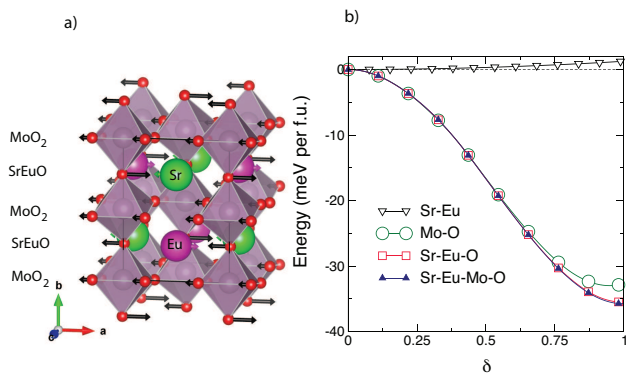


FIG. 1. (Color online) a) DFT relaxed crystal structure of SEMO in $Imm2$ ferroelectric crystal symmetry with polar displacements along the $[100]$ -direction. b) Total energy gain (per formula unit, f.u.) as a function of ionic displacement given as a percentage present in the equilibrium structure (δ). Energy of the full mode is compared to that of the partial modes, where a reduced set of atoms are displaced (see legend).

with half-filled shells follows the longstanding Mott-Hubbard paradigm, materials with integer d -orbital occupation that are different from half-filling (like d^2 and d^4 configurations which *partially* fill the three t_{2g} bands) and a sizable Hund's coupling display unexpected properties. These features have led to a class of materials, dubbed 'Hund's metals', where sizable electron-electron correlations exist even for moderate values of the Coulomb repulsion very far from the critical value of the Mott transition [14, 22]. However, the extent to which the Hund's interaction can drive a correlated metallic state compatible with ferroelectric-like displacements is unknown.

In this Letter, we demonstrate the possibility to engineer polar distortions in a 'Hund's metal', proposing $SrEuMo_2O_6$ (SEMO) as a new compound. To characterize this material and its electronic properties, we use a combination of density functional theory (DFT) and dynamical mean-field theory (DMFT) [23]. Utilizing DFT calculations, we first show that the ordered molybdate exhibits a polar metallic ground state, fulfilling the structural criterion described in Ref. 7. We then establish with our DFT+DMFT approach that SEMO is in proximity to region of phase space exhibiting bad metallic behavior driven and stabilized by the Hund's coupling owing to the d^2 electronic configuration in the Mo $4d$ manifold. The enhanced electron correlations that characterize the poor-metallic state reduce the ability of the metal to screen the ferroelectric-like distortions, leading to a 'ferroelectric' metallic state. Our finds indicate that electronic configurations conducive to Hund's-metal behavior may be a promising arena for the discovery of yet unknown noncentrosymmetric metals.

A promising route to lift inversion symmetry and realize a NCSM is to use cation ordering in combination with non-polar cooperative displacements [7]; the former being experimentally accessible through either syn-

thetic bulk chemistry routes or heteroepitaxial thin film growth [24, 25]. With this in mind, we select $SrMoO_3$ (SMO) and $EuMoO_3$ (EMO) with d^2 electronic configurations and nearly identical pseudo-cubic lattice constants ($a=3.975$ Å) [26, 27]. We then construct a $1/1$ period superlattice of SMO and EMO in which the Sr and Eu cations are arranged in a rock-salt structure (see Fig. 1a) and the in-plane lattice parameters are fixed to the pseudo-cubic lattice constant, $a=c=3.975$ Å. This cation ordering should be experimentally accessible via growth on a (111) terminated perovskite substrate.

Next variable-volume atomic relaxations along the b direction are performed starting from a centrosymmetric $I4/mmm$ symmetry with spin-polarized DFT calculations within the generalized-gradient approximation (PBE) [28] as implemented in the Vienna *Ab initio* Simulation Package (VASP) [29] with the projector augmented wave (PAW) method [30, 31]. Spin-polarized calculations for SEMO lead to a non-magnetic ground state, consistent with that of bulk SMO and EMO.

We determine the most stable ionic configuration to be polar with $Imm2$ symmetry and 35 meV per formula unit (f.u.) lower in energy than the centric $I4/mmm$ phase [32]. The octahedral tilt pattern of SMO and EMO is $a^0a^0a^0$ and $a^0a^0c^-$, respectively, whereas in SEMO we find the $a^-b^+a^-$ tilt with a^- and b^+ rotations of 4° and 0.11° , respectively. The loss of inversion symmetry is a consequence of the out-of-phase octahedral tilt modes (see Fig. 1a), which allow for anti-polar Sr and Eu cation displacements connected with neighboring O sites [33]. (Note that if the b^+ tilt amplitude is zero, the structure remains polar owing to the out-of-phase rotations that in combination with the rock salt Sr and Eu order lift inversion.) Along the polar a axis (see Fig. 1a) we find (i) Sr and Eu ions have opposite displacements of respectively $0.045, -0.018$ Å (ii) apical O ions belonging to the same octahedra displace 0.33 and -0.28 Å while planar O ions displace by -0.020 Å and (iv) the Mo cations have negligible ferroelectric displacements. The situation along the non-polar b and c axes is different: the Sr, Eu and apical O ions do not displace while the planar O sites exhibit antipolar displacements.

In Fig. 1b we show the variation of the total energy as a function of the amplitude δ of atomic displacements for the different atoms involved in the distortion mode connecting the centrosymmetric ($\delta = 0$) structure to the polar ground state ($\delta = 1$). We compare the total mode involving all ions (Sr-Eu-Mo-O) with three partial displacements: A-cation only mode (Sr-Eu), A-O mode (Sr-Eu-O) that includes the displacement of Sr, Eu and O atoms, and the B-O mode (Mo-O) whereby the Sr and Eu displacements are neglected. As expected, the largest energy gain is obtained when all atoms are included (Sr-Eu-Mo-O, Fig. 1b). Since Mo cations remain largely centered in the octahedra, the results for the Mo-O mode show that oxygen displacements are essential to the

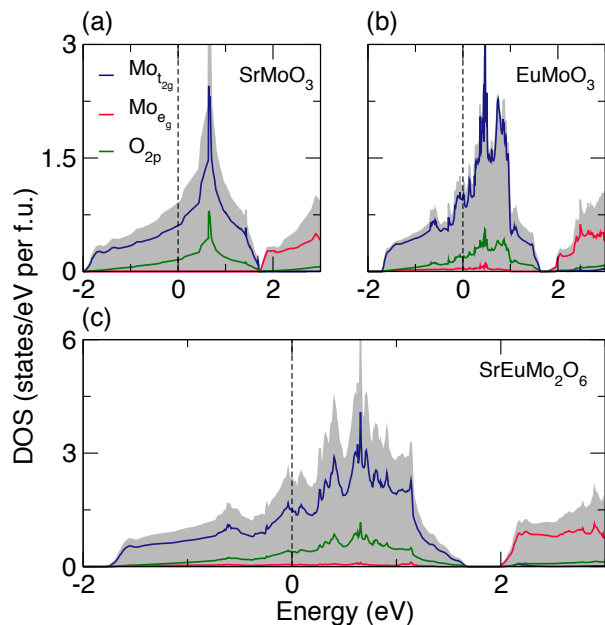


FIG. 2. (Color online) Atom- and orbital-resolved density of state for SMO (a), EMO (b) and SEMO (c) at the DFT-PBE level. The energy zero is set to the Fermi level.

structure stability; indeed, the polar Sr-Eu displacements alone lead to an increase in energy in the absence of O displacements (Sr-Eu, Fig. 1b). The difference between the total mode and that which omits the Mo displacements (Sr-Eu-O, Fig. 1b) demonstrates that the ferroelectric ordering is stabilized by cooperative and coupled displacements of the Sr, Eu and O ions. We note that among all the O atoms the main contribution is due to apical anions found in the AO monoxide planes (Fig. 1a). The stability of these polar displacements depends on the delicate balance between electrostatic interactions of the local dipole moments they generate and the electronic screening effects in the crystal. We now consider the electronic properties of SEMO to address the role of screening.

In Fig. 2 we compare the density of states (DOS) calculated within DFT-PBE for bulk SMO and EMO to that of SEMO. The DOS of SMO and EMO are rather similar [34]: Both bulk molybdates are found to be metallic with the extended Mo 4d states dispersing from approximately -2 eV to 1.8 eV above the Fermi level (E_F). As shown in panel (c), SEMO is also a metal with sizable spectral weight at E_F . The low-energy contribution to the spectral density is dominated by the bands arising from the Mo 4d² electrons, which are weakly entangled with the oxygen 2p states mainly distributed from -8 eV to -4 eV below E_F (not shown). The 4d bands in SEMO have an overall width of 3.4 eV, which is reduced with respect to SMO and EMO owing to the increased tilting of the MoO₆ octahedra. The narrowing of the t_{2g} manifold also separates it from the higher-lying e_g bands.

Next we evaluate the screening behavior of the low-

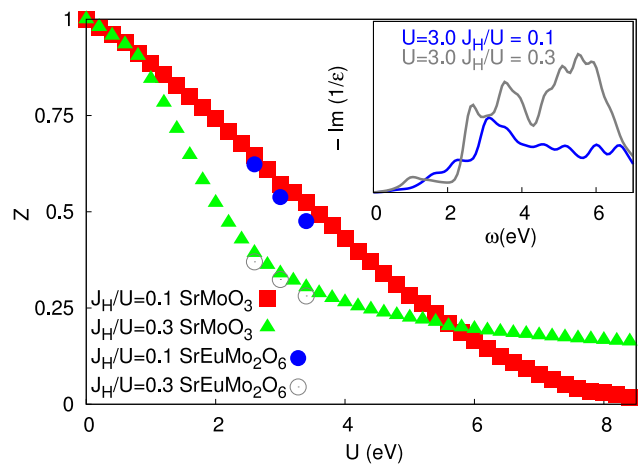


FIG. 3. (Color online) Quasiparticle weights (Z) calculated within DFT+DMFT for SMO, EMO and SEMO at different values of the ratio J_H/U . Inset: Imaginary part of the inverse dielectric function, $1/\epsilon$, for SEMO at different J_H/U values.

energy conducting electrons (Fig. 3), investigating first electronic correlations in bulk SMO and then comparing its behavior with the SEMO superlattice. (Data for EMO is not shown because of the similarities in the results). In order to include the on-site Coulomb interaction parameterized by the Hubbard U and the Hund's coupling J_H in our DMFT calculations (we use a Kanamori parametrization), we compute maximally-localized Wannier orbitals [35] for the 4d Mo states over the energy range spanned by the t_{2g} orbitals across E_F to construct the non-interacting part of our Hamiltonian. In the DFT+DMFT scheme [23], which treats the lattice problem as an impurity embedded in a self-consistent bath, we employ Exact Diagonalization (ED) [36, 37] as the impurity solver using an Arnoldi algorithm [38] to perform the diagonalization.

To characterize the degree of correlation of the system we study the quasiparticle weight Z , which is 1 for a non-interacting metal and decreases as a function of the interaction strength. A vanishing Z signals a Mott insulating phase. The constrained random-phase approximation (cRPA) for bulk SMO gives $U = 3.0$ eV and $J_H = 0.3$ eV [39]. In Fig. 3 we plot Z as a function of U for two values of the ratio J_H/U ($J_H/U = 0.1$, which corresponds to the cRPA values, and 0.3). For bulk SMO with cubic symmetry the t_{2g} orbitals are perfectly degenerate and occupied by 2/3 electrons per orbital and the states share the same value of Z . For the cRPA value of $J_H/U = 0.1$, we find $Z \simeq 0.6$, consistent with experiment and previous theoretical estimates [40].

The evolution of Z follows the behavior discussed in Ref. 22, where a rapid decrease for small U is followed by a flattening of the $Z(U)$ curve, and ultimately to a Mott transition, which occurs at a relatively large value of U (~ 8 eV for $J_H/U = 0.1$). This behavior is more pronounced with increasing J_H/U with a faster initial

decrease and a much slower decrease to an enhanced critical strength. For the cRPA estimates, we find that SMO is indeed on the brink of a ‘Hund’s correlated’ phase and far from the Mott state, which would require an unphysical enhancement of the ratio between U and the bare kinetic energy.

We now turn to SEMO, where the loss of inversion symmetry alters the t_{2g} manifold symmetry through a small crystal-field splitting and a change in the local hybridization, leading to small differences between the Z values for the different orbitals. For the sake of simplicity, we plot the orbital-averaged Z , and note that the reduced symmetry introduces minor modulations of the orbital occupancies without changing the physical picture. Here we observe a small reduction of the quasiparticle weight Z and consequently a slight increase of the degree of correlation (see the data plotted as circles in Fig. 3), which pushes SEMO towards a correlated regime driven by the Hund’s coupling. Therefore the polar metallic state of SEMO is characterized by the simultaneous presence of polar distortions and a poor metallic behavior with intermediate electronic correlation strength. Indeed, the correlated nature of the metallic state in bulk SMO is evidenced experimentally by a low quasiparticle coherence scale around $T^* = 140$ K [41], which is of the same order as Sr_2RuO_4 [42] above which highly incoherent conduction characterizes the system. Based on our DMFT calculations, we expect similar behavior for SEMO. Above T^* the incoherent conduction electrons would contribute even less to the screening of local dipole moments formed by the polar lattice mode, further favoring the coexistence of the broken inversion symmetric state and metallicity.

To further justify this argument, we also plot the contribution of the Mo $4d$ electrons to the frequency-dependent imaginary part of the inverse dielectric function ($1/\epsilon$) for SEMO, which directly captures the effects of screening (Fig. 3, inset) [43]. Although the full screening of the Coulomb interactions in a crystal is due to contributions from all orbitals, *e.g.*, including those of the ligands, we find that in correlated SEMO the contribution from the conduction orbitals is strongly reduced owing to electron-electron correlations which are strongly enhanced by increasing the Hund’s coupling. On average $\Im(1/\epsilon)$ is larger for $J_H = 0.3$ eV in the more correlated regime owing to the reduced Z derived from Hund’s assisted correlations. Both features give a reduction to dielectric screening and in part alleviates the incompatibility between metal and ferroelectric-like orders.

The present study, together with previous indications of strong correlations in LiOsO_3 [8] and other NCSM, suggests that materials with d^2 or d^4 configurations are promising candidates from which to realize new polar metals. Provided ferroelectric-like displacements can be realized through a lattice instability, poor screening of the electric dipoles will be provided in the correlated metallic state when the Hund’s coupling is sufficiently large. An

interesting example could be given by LiReO_3 , which displays the same polar crystal class as LiOsO_3 ($R3c$) [44] owing to the off-centering of Li ions, while it shares the same nominal d^2 electronic configuration of SEMO. Finally we also remark that the proposed ultra-short NCSM ruthenate $(\text{SrRuO}_3)_1/(\text{CaRuO}_3)_1$ superlattices have a d^4 Ru^{4+} configuration [7]. The ruthenate electronic structure, analogously to the d^2 of SEMO, is ideal for Hund’s metal physics, as has been discussed for the bulk end-members [21, 45]. Therefore the electronic stability of the NCSM state in this superlattice may be supported by the same mechanism described herein, *i.e.*, poor metallicity assisted by Hund’s coupling.

In summary, we propose $\text{SrEuMo}_2\text{O}_6$ as polar Hund’s metal. Our electronic structure calculations reveal that the polar structure is driven by asymmetric displacements of the ions in the SrO and EuO planes, which occur with ferromagnetic ordering of spins on the Mo ions. The ferroelectric-like state coexists with a correlated metallic phase which relies on the Hund’s coupling and it is robust with respect to Mott localization. The poorly coherent quasiparticles are ineffective at completely screening the ordered local dipole moments. These results strengthen the link between correlated metallic states and the propensity of a metallic material to adopt polar structure, facilitating the selection or design of new correlated polar metals for enhanced magnetoelectronic responses or customized antisymmetric exchange interactions, which support exotic magnetic textures (helical or skyrmionic structures). Although our current understanding of polar metals reveals that most of them are in a correlated electronic regime with bad metallic behavior, we do not eliminate the possibility that non-correlated polar metals may exist; rather, strong electronic correlations appears to be a favorable ingredient to stabilizing noncentrosymmetric metallic phases, but it may not be a prerequisite in scenarios where the inversion lifting displacements are indeed decoupled from the low-energy electronic structure.

G.G. and M.C. acknowledge financial support from the European Research Council under FP7/ERC Starting Independent Research Grant “SUPERBAD” (Grant No. 240524). D.P. and J.M.R. acknowledge the Army Research Office for financial support (Grant No. W911NF-15-1-0017), and the HPCMP of the DOD and XSEDE supported by NSF (Grant No. OCI-1053575) for providing computational resources.

* ggiovann@sissa.it

† jrondinelli@northwestern.edu

- [1] V. Keppens, Nat. Mater. **12**, 952 (2013).
- [2] Anderson and Blount, Phys. Rev. Lett. **14**, 217 (1965).
- [3] Y. Shi, Y. Guo, X. Wang, A. J. Princep, D. Khalyavin, P. Manuel, Y. Michiue, A. Sato, K. Tsuda, S. Yu, M. Arai, Y. Shirako, M. Akaogi, N. Wang, K. Yamaura and A. T.

- Boothroyd, Nat. Mater. **12**, 1024 (2013).
- [4] W. Cochran, Adv. Phys., 9 (1960) 387.
- [5] X. Gonze, J.-C Charlier, D. C. Allan and M. P. Teter, Phys. Rev. B, 50 (1994) 13035.
- [6] Ph. Ghosez, X. Gonze and J.-P. Michenaud, Europhys. Lett. 33 713 (1996).
- [7] D. Puggioni and J. M. Rondinelli, Nat. Commun. **5**, 3432 (2014).
- [8] G. Giovannetti and M. Capone, Phys. Rev. B **90**, 195113 (2014).
- [9] K. Poeppelmeier, J. Thiel, J. Vaughey, M. Anderson, M., D. Groenke, C. Stern, B. Dabrowski, D. Hinks and A. Mitchell, Physica C: Superconductivity 185, Part 1, 525 (1991).
- [10] J. T. Vaughey, J. P. Thiel, E. F. Hasty, D. A. Groenke, C. L. Stern, K. R. Poeppelmeier, B. Dabrowski, D. G. Hinks and A. W. Mitchell, Chem. Mat. 3, 935 (1991).
- [11] A. Sergienko, V. Keppens, M. McGuire, R. Jin, J. He, S. H. Curnoe, B. C. Sales, P. Blaha, D. J. Singh, K. Schwarz, and D. Mandrus, Phys. Rev. Lett. **92**, 065501 (2004).
- [12] J. C. Petersen, M. D. Caswell, J. S. Dodge, I. A. Sergienko, J. He, R. Jin and D. Mandrus, Nat. Phys. **2**, 605 (2006).
- [13] X. Deng, J. Mravlje, R. Zitko, M. Ferrero, G. Kotliar, and A. Georges, Phys. Rev. Lett. 110, 086401 (2013)
- [14] A. Georges, L. de' Medici, and J. Mravlje, Annu. Rev. Condens. Matter Phys. **4** 137 (2013).
- [15] K. Haule and G. Kotliar, New J. Phys. **11**, 025021 (2009)
- [16] Y. Wang, X. Liu, J. D. Burton, S. S. Jaswal, and E. Y. Tsybal, Phys. Rev. Lett. **109**, 247601 (2012).
- [17] T. Kolodiazny, M. Tachibana, H. Kawaji, J. Hwang, and E. Takayama-Muromachi, Phys. Rev. Lett. **104**, 147602 (2010).
- [18] J. Hwang, T. Kolodiazny, J. Yang, and M. Couillard, Phys. Rev. B **82**, 214109 (2010).
- [19] N. Trivedi and M. Randeria, Phys. Rev. Lett. **75**, 312 (1995).
- [20] N. L. Wang, J. J. McGuire, T. Timusk, R. Jin, J. He, and D. Mandrus, Phys. Rev. B **66**, 014534 (2002).
- [21] J. Mravlje, M. Aichhorn, T. Miyake, K. Haule, G. Kotliar, and A. Georges, Phys. Rev. Lett. **106**, 096401 (2011).
- [22] L. de' Medici, J. Mravlje, and A. Georges, Phys. Rev. Lett. **107**, 256401(2013).
- [23] A. Georges, G. Kotliar, W. Krauth, and M. J. Rozenberg, Rev. Mod. Phys. **68**, 13 (1996).
- [24] G. King, P. M. Woodward, J. Mater. Chem. **20**, 5785 (2010); W. Dachraoui, T. Yang, C. Liu, G. King, J. Hadermann, G. Van Tendeloo, A. Llobet, A. and M. Greenblatt, Chem. Mat. **23**, 2398 (2011).
- [25] P. Zubko, S. Gariglio, M. Gabay, P. Ghosez, J. M. Triscone, Annu. Rev. Condens. Matter Phys. 2, 141 (2011).
- [26] Y. Kozuka, H. Seki, T. C. Fujita, S. Chakraverty, K. Yoshimatsu, H. Kumigashira, M. Oshima, M. S. Bahrany, R. Arita, and M. Kawasaki, Chem. Mater., **24**, 3746 (2012).
- [27] R. B. Macquart, B. J. Kennedy, and M. Avdeev, J. Solid State Chem. **183**, 249 (2010).
- [28] J. P. Perdew, K. Burke, and M. Ernzerhof, Phys. Rev. Lett. **77**, 3865 (1996).
- [29] G. Kresse and J. Hafner, Phys. Rev. B, **47**, 558 (1993); G. Kresse and J. Hafner, Phys. Rev. B, **49**, 14251 (1994); G. Kresse and J. Furthmuller, Comput. Mat. Sci., **6**, 15 (1996); G. Kresse and J. Furthmuller, Phys. Rev. B **54**, 11169 (1996).
- [30] P. E. Blöchl, Phys. Rev. B **50**, 17953 (1994); G. Kresse and D. Joubert, Phys. Rev. B **59**, 1758(1999).
- [31] A kinetic cutoff energy of 550 eV is used to expand the wavefunctions and a Γ centered $10 \times 8 \times 10$ k -point mesh combined with the tetrahedron method is used for Brillouin zone integrations. Atomic relaxations are continued until the changes in the total energy are less than 10^{-8} eV.
- [32] Using the lattice vectors: $(a, b, c) = (5.621, 7.983, 5.621)$ Å, the optimized Wyckoff positions are: Sr: $2a, z = 0.497$; Eu: $2b, z = 0.508$; Mo: $4d, y = 0.75, z = 0$; O(1): $8e, x = 0.747, y = 0.778, z = 0.246$; O(2): $2b, z = 0.059$; and O(3): $2a, z = -0.246$.
- [33] J. Young and J. M. Rondinelli, Chem. Mater. **25**, 4545 (2013).
- [34] The f electrons of Eu are kept frozen in our DFT calculations being localized at 2 eV below the Fermi level in the calculations of EuMoO₃ [26].
- [35] A. A. Mostofi, J. R. Yates, Y.-S. Lee, I. Souza, D. Vanderbilt and N. Marzari, Comput. Phys. Commun. **178**, 685 (2008).
- [36] M. Caffarel and W. Krauth, Phys. Rev. Lett. **72**, 1545 (1994).
- [37] M. Capone, L. de' Medici, and A. Georges, Phys. Rev. B **76**, 245116 (2007).
- [38] R. B. Lehoucq, D. C. Sorensen, and C. Yang, ARPACK Users Guide (SIAM, Philadelphia, 1997).
- [39] L. Vaugier, H. Jiang, and S. Biermann, Phys. Rev. B **86**, 165105 (2012).
- [40] H. Wadati, K. Yoshimatsu, H. Kumigashira, M. Oshima, T. Sugiyama, E. Ikenaga, A. Fujimori, J. Mravlje, A. Georges, A. Radetnac, K. S. Takahashi, M. Kawasaki, Y. Tokura, Phys. Rev. B **90**, 205131 (2014).
- [41] I. Nagai, N. Shirakawa, S-I. Ikeda, R. Iwasaki, H. Nishimura and M. Kosaka, Appl. Phys. Lett. **87**, 024105 (2005).
- [42] S.-C. Wang, H.-B. Yang, A. K. P. Sekharan, H. Ding, J. R. Engelbrecht, X. Dai, Z. Wang, A. Kaminski, T. Valla, T. Kidd, A. V. Fedorov, and P. D. Johnson, Phys. Rev. Lett. **92**, 137002 (2004).
- [43] The imaginary part of the dielectric function is obtained from the DMFT optical conductivity $\sigma(\omega)$ as $\epsilon_2(\omega) = 4\pi\sigma(\omega)/\omega$, and the real part may be obtained via the Kramers-Kronig relation to provide the full complex dielectric function.
- [44] R.J. Cava, A. Santoro, D.W. Murphy, S.M. Zahurak, R.S. Roth, J. Solid State Chem. **42**, 251 (1982).
- [45] D. Stricker, J. Mravlje, C. Berthod, R. Fittipaldi, A. Vecchione, A. Georges, and D. van der Marel, Phys. Rev. Lett. **113**, 087404 (2014)